Title
RKKY Exchange Bias Mediated Ultrafast All-Optical Switching of a Ferromagnet

Journal
Advanced Functional Materials, 32(8)

ISSN
1616-301X

Authors
Chatterjee, Jyotirmoy
Polley, Debanjan
Pattabi, Akshay
et al.

Publication Date
2022-02-01

DOI
10.1002/adfm.202107490

RKKY exchange bias mediated ultrafast all-optical switching of a ferromagnet

Jyotirmoy Chatterjee[1*], Debanjan Polley[1,2], Akshay Pattabi[1], Hyejin Jang[1,#], Sayeef Salahuddin[1] and Jeffrey Bokor[1,2]

[1]*Department of Electrical Engineering and Computer Sciences, University of California, Berkeley, California 94720, USA*
[2]*Lawrence Berkeley National Laboratory, 1 Cyclotron Road, Berkeley, California 94720, USA*

The discovery of ultrafast helicity-independent all-optical switching (HI-AOS) as well as picosecond all electrical switching of a ferrimagnet inspired the ultrafast spintronic community to investigate ultrafast switching of a ferromagnet either by exchange or by a non-local spin transport mechanism for realizing an ultrafast storage and memory device. In this manuscript, we demonstrate exchange mediated HI-AOS of an Ruderman-Kittel-Kasuya-Yosida (RKKY) exchange coupled [Co/Pt]-multilayers/Pt spacer/CoGd heterostructure. We studied layer-resolved static magnetic properties and single shot HI-AOS to demonstrate ultrafast switching of Co/Pt multilayers when ferromagnetically or antiferromagnetically coupled with CoGd. Time-resolved magnetization dynamics show switching of the Co/Pt in 3.5 ps, which is the fastest switching of a ferromagnet reported to date. Employing an extended microscopic three-temperature model, we simulate the temporal dynamics of the exchange coupled ferromagnet-ferrimagnet heterostructure, qualitatively and quantitatively explaining the experimental switching phenomena. This work experimentally as well as theoretically establishes the mechanism of exchange mediated all-optical switching of ferromagnet-ferrimagnet heterostructures. This type of heterostructure can be integrated with a magnetic tunnel junction for efficient reading after ultrafast energy-efficient switching.

*At present: Fraunhofer IPMS, An der Bartlake 5, 01109 Dresden, Germany
#Materials Science and Engineering, Seoul National University, Seoul 08826, Republic of Korea

Ever since the discovery of ultrafast all-optical demagnetization[1] and magnetization reversal phenomena,[2–4] there has been a strong interest in realizing ultrafast energy-efficient non-volatile spintronic memory and storage devices. Picosecond magnetization reversal phenomena, by femtosecond optical pulses and/or electronic pulses[5] are expected to be energy efficient and therefore believed to be an alternative ultrafast memory technology[6,7] to address the exponential growth of data and computing demand in this decade. One of the important discoveries in the field of ultrafast optical control of magnetism is the helicity independent all-optical switching (HI-AOS) with a single laser pulse.[3,4] However, so far this magnetization reversal through a non-equilibrium thermal excitation of magnetization is mainly observed in Gd based ferrimagnets (GdFeCo,[4] CoGd,[8] GdTbCo[9] alloy and Co/Gd bilayers[10]), ferrimagnetic Co/Tb multilayers[11] and ferrimagnetic Mn_2Ru_xGa Heusler alloy.[12] Also, an optically switchable magnetic tunneling junction (MTJ) was demonstrated employing GdFeCo as the storage layer.[13] However, in that case, due to low spin polarization, the tunneling magnetoresistance ratio (TMR) was too small (~0.6 %) for practical applications. Thus, it is of great interest to switch a ferromagnet with helicity independent optical pulses, which could then be implemented as a storage layer in a high TMR memory cell.

Up until now, two routes of HI-AOS switching of a ferromagnet have been demonstrated using magnetic heterostructures containing both a ferrimagnetic and a ferromagnetic layer. One mechanism is to exploit spin polarized current transport.[14] In this case, the spin current generated due to the ultrafast switching of GdFeCo under optical excitation is responsible for the switching of Co/Pt multilayers in the same stack. The other mechanism is Ruderman-Kittel-Kasuya-Yosida (RKKY) exchange coupling mediated HI-AOS of a ferromagnet.[11,15] On this particular platform, 7 ps switching speed of a Co/Pt multilayer has been demonstrated when it was ferromagnetically exchange-coupled with a GdFeCo ferrimagnet.[15] However, GdFeCo does not maintain perpendicular magnetic anisotropy (PMA) for a patterned dot with a diameter much less than 1 μm.[8] Hence, GdFeCo is not a desirable choice for building a coupled ferromagnet-ferrimagnet heterostructure as a storage layer of a nano-patterned memory cell. On the other hand, CoGd ferrimagnet layer can maintain PMA, when it is patterned down to below 200 nm diameter.[8]

Therefore, in this work, we have investigated the static magnetic properties, all-optical switching and time-resolved magnetization dynamics of a CoGd/Pt-spacer/[Co/Pt]-multilayer heterostructure. We demonstrate that the indirect RKKY exchange coupling between the CoGd-ferrimagnet and Co/Pt MLs-ferromagnet depends on a Pt spacer thickness. The multilayers exhibit HI-AOS for both ferromagnetic and antiferromagnetic coupling. The switching speed of the ferromagnet is about 3 ps. To the best of our knowledge, this is the fastest switching of a ferromagnet ever reported with any mechanism, including AOS, spin-transfer torque and spin-orbit torque.[16] Moreover, a theoretical understanding of indirect RKKY exchange coupling mediated HI-AOS is still lacking. In order to delve into the microscopic mechanism of magnetization reversal of Co/Pt MLs and both sublattices of the CoGd alloy, we performed analytical calculations extending the microscopic three-temperature model (M3TM).[17,18] Considering inter-sublattice, intra-sublattice and indirect RKKY exchange scatterings, we explain the magnetization reversal dynamics of different magnetic components of ferromagnetically and antiferromagnetically coupled or decoupled ferromagnet-ferrimagnet heterostructures. The calculated values of switching times are in agreement with experimental observations.

Results and Discussion

Sample structure and magnetic metrology. The schematic of the ferromagnet-ferrimagnet heterostructures used for this experiment is shown in **Figure 1**. The Co/Pt multilayers and the CoGd ferrimagnetic alloy are separated by a Pt spacer layer. The atomic composition of CoGd is expected to be $Co_{69.3}Gd_{30.7}$, which is calculated from the deposition rate of Co and Gd as described in Section S1 of supporting information. The easy-axis of both CoGd and Co/Pt layers are along the out-of-plane direction. The pink and blue color arrows respectively represent the net magnetization directions of the CoGd alloy and Co/Pt multilayers. The thickness of the Pt spacer is varied from 1 nm to 4.5 nm in steps of 0.5 nm, which essentially changes the strength and/or nature of RKKY exchange coupling between the two adjacent magnets. Accordingly, the magnetization reversal process of the two magnetic layers from one saturation direction to the opposite direction, for example from the positive-saturation (both the magnetizations are pointed along positive field direction) to negative-saturation (both the magnetizations are pointed along negative field direction) and vice-versa under the application of magnetic field also changes. In order to understand the type of RKKY coupling and calculate the coupling strength between the CoGd ferrimagnet and Co/Pt multilayers for different Pt spacer thickness, hysteresis loops were measured by magneto-optical Kerr effect (MOKE) microscopy. The coupling is ferromagnetic for the Pt thickness of 1 to 2 nm, which is manifested by the single-step hysteresis loops shown in

Figure 2c-e. The coupling becomes antiferromagnetic for 2.5 and 3 nm Pt-spacers. As a result, we observe two- or three-step magnetization reversal from positive saturation to negative saturation and vice-versa (see Figure 2a,b). The minor loop in red color describes the magnetization reversal of CoGd. The shift of this minor loop is indicative of the exchange bias field or RKKY coupling strength. The exchange bias of CoGd with the Co/Pt multilayer are respectively 1160 Oe and 100 Oe for 2.5 and 3 nm Pt spacer thicknesses. As exchange bias is large for 2.5 nm Pt-spacer, the maximum field of MOKE microscopy tool was not sufficient for measuring the hysteresis loop of this sample. Therefore, we measured magnetization versus field (M(H)) hysteresis loop of this particular sample by vibrating sample magnetometry (VSM). Notably, therefore, the symmetry of the magnetic hysteresis loop of the stack with Pt 2.5 nm spacer is different than that of the 3 nm. Moreover, a three-step reversal process is observed due to larger RKKY exchange bias.[19] The magnetization of the CoGd derived from the M(H) loop is 106 emu/cm^3. Therefore, the RKKY coupling energy ($E_{ex}= H_{ex}M_{s\text{-}CoGd}t_{CoGd}$) energy are 0.123 and 0.01 erg/cm^2 respectively for 2.5 nm and 3 nm Pt spacers. The ferrimagnet and ferromagnet become decoupled for the Pt spacer thickness of 3.5 nm and above. The MOKE hysteresis loops shown in Figure 2f and g, are for the heterostructures with 3.5 nm and 4 nm Pt thickness. The CoGd minor loops shown by red color for these spacer thicknesses are centered to zero field indicating zero coupling between the CoGd and Co/Pt MLs.

Single-shot all-optical switching.

We now discuss experiments to investigate whether the ferromagnet layer can be optically switched for both ferromagnetic and antiferromagnetic RKKY coupling to the CoGd layer as well as for decoupling. First, single-shot switching experiments are presented. The samples were irradiated with a single 80 fs (full-width-half-maximum) linearly polarized laser pulse (central wavelength of 800 nm) and the magnetization state detected with MOKE microscopic imaging using a 630 nm light-emitting diode light source. The initial condition of different samples, before the optical pulse, are set by fully saturating the magnetizations of both the magnetic layers along the positive field direction and then turning off the magnetic field. At the starting condition, the magnetizations of both the CoGd and Co/Pt MLs are magnetized along the up-direction for ferromagnetically coupled samples. After the first pulse, both the magnetizations are reversed to the down direction. The magnetization toggles from up-up to down-down to up-up configurations with consecutive optical pulses as shown by the images of Figure 2j-l. For antiferromagnetically coupled samples, the magnetizations of Co/Pt MLs and CoGd are respectively set along up and down direction (up-down) as the starting condition. The magnetization toggles from up-down to down-up to up-down configuration with successive laser pulses as presented by the images of Figure 2h,i. Therefore, single-shot HI-AOS of the ferromagnet (Co/Pt MLs) is observed for both ferromagnetically and antiferromagnetically coupled samples, which is confirmed after analyzing the images. The image analysis is explained in section-S2. In contrast, for decoupled samples (Pt spacer ≥ 3.5 nm), only the CoGd undergoes HI-AOS. The magnetization of Co/Pt MLs is not switched. As a result, we see darker contrast at the center of the image (see Figure 2m,n), where the pulse is irradiated, which is in agreement with the reversal step of CoGd as evident from the MOKE hysteresis loops shown in the Figure. 2f,g.

Depth resolved single-shot all-optical switching:

In order to directly capture the images of quasi-static magnetization states after single-shot AOS of the individual magnetic layer, for example, either of the CoGd alloy or of the Co/Pt MLs, the samples were characterized by the layer sensitive MOKE microscopy technique. A quarter-wave plate (QWP) is placed in the optical path after the polarizer to establish the additional depth sensitive magnetic probing[15,20–22] for characterizing the layer selective MOKE hysteresis loops (see Figure 3a-c) or depth-sensitive imaging after single-shot HI-AOS (see Figure 3d-f). In this technique, the MOKE signal is a mixture of Kerr rotation and Kerr ellipticity, which is tuned by the angle of QWP. It is possible to determine an angle at which the amplitude of Kerr signal coming from one magnetic layer is nulled out. Therefore, only the Kerr signal from the other magnetic layer contributes in the MOKE signal. We start with the decoupled or anti-ferromagnetically coupled samples and find the two QWP angles at which the Kerr signals are respectively originated from the CoGd and from the Co/Pt MLs. Similar angles of the QWP remain valid irrespective of the thickness of the Pt spacer for depth sensitive magnetic and AOS characterization, because the Kerr signal only originates from a magnetic layer. Moreover, the total penetration depth of 630 nm and 800 nm light is more than 20 nm,[15,23] which is also shown by the absorption profile in Figure S3 of the supplementary information. Note that the absorption profiles are calculated by the transfer matrix method described in section S3.

The depth-sensitive hysteresis loops are presented in Figure 3a-c for decoupled, antiferromagnetically coupled and ferromagnetically coupled samples. The hysteresis loops clearly show the MOKE signal is either originating from CoGd or from Co/Pt MLs. Similar to the loops shown in Figure 2, a zero and a positive bias field is observed in the minor loops of CoGd for decoupled and antiferromagnetically coupled samples. On the other hand, similar coercivity of the CoGd-alloy and Co/Pt MLs for 1 nm Pt-spacer again supports ferromagnetic coupling between them. After setting up the above-mentioned depth sensitivity, a direct imaging of toggle switching of the CoGd alloy and of the Co/Pt MLs, by a single optical pulse is shown in Figure 3d-f. Figure 3d reveals that only the magnetization of CoGd is reversed with femtosecond laser pulse and Co/Pt MLs undergoes a partial demagnetization. On the contrary, both the CoGd ferrimagnet and the Co/Pt ferromagnet are reversed for both ferromagnetic and antiferromagnetic couplings (see Figure 3e,f). In previous work,[14,24] it was shown that Pt spacer thicker than 2 nm almost fully blocks the non-local spin current, generated due to the ultrafast switching of CoGd which can reverse the magnetization of Co/Pt. But here we have demonstrated the switching of Co/Pt MLs for 3 nm thick Pt spacer. Moreover, non-local spin current will only switch the magnetization of the Co/Pt MLs when its magnetization is oppositely aligned with respect to the magnetic moment of the Gd-sublattice of the CoGd alloy.[14] This is because spin current generated from Gd is responsible to switch the ferromagnet on the other side of spacer layer. In contrast, here we have demonstrated the switching of Co/Pt MLs for both ferromagnetic and antiferromagnetic coupling when the magnetization of Co/Pt MLs are respectively aligned opposite to and along the direction of the Gd-sublattice's magnetization. Hence, we rule out the possibility of switching of the Co/Pt multilayer triggered by non-local spin current generated by the switching of CoGd. The spin current can also be generated due to spin-dependent Seebeck effect (SDSE) due to the possible thermal gradient present across the layers.[25] However, for CoGd the contribution of spin current generation during initial nonequilibrium state, is expected to be dominated by the demagnetization of CoGd. The contribution of spin current from SDSE is expected to be much smaller in magnitude compared to the spin current originated due to demagnetization.[26] Moreover, if the temperature gradient is playing any role in the observed switching, it cannot explain the switching of Co/Pt multilayers for both ferromagnetically and antiferromagnetically coupled stacks. Dipolar stray fields coming from the CoGd alloy acting on the demagnetized Co/Pt MLs is also not responsible as it cannot explain all the different switching scenarios, for example up-up to down-down and vice versa for ferromagnetically coupled samples, up-down to down-up and vice versa for anti-ferromagnetically coupled samples and non-reversal of Co/Pt multilayers' magnetization for decoupled samples. Hence, we conclude that the switching mechanism must be RKKY exchange coupling mediated AOS of Co/Pt MLs.

Layer-sensitive time-resolved magnetization dynamics:

We next present data on the ultrafast magnetization dynamics of the various samples. In order to probe temporal dynamics of the Co/Pt ML and CoGd layer, we performed stroboscopic pump-probe measurements with an 800 nm laser using the time-resolved magneto optical Kerr effect (TR-MOKE) technique. We again use a QWP for establishing layer sensitivity with either of the magnetic layers, which is confirmed by measuring hysteresis loops by MOKE using the 800 nm laser probe beam. Figure S4B exhibits layer-sensitive laser-MOKE hysteresis loops, which are in agreement with the layer-sensitive hysteresis loops measured by MOKE microscopy technique as shown in Figure 3a-c.

The temporal dynamics of the decoupled sample is depicted in Figure 4a. The dynamics clearly shows HI-AOS of the CoGd alloy after ~1.5 ps. However, the Co/Pt multilayer is only partially demagnetized following a slow remagnetization along its initial magnetization direction. In contrary to the decoupled sample, the ferromagnetically coupled sample exhibits switching of both the CoGd alloy and Co/Pt multilayer as shown in Figure 4b. CoGd reverses its magnetization after ~1.5 ps. The Co/Pt multilayer exhibits switching after only 3 ps. To the best of our knowledge this is the fastest switching of a ferromagnet ever reported irrespective of the stimuli (STT, SOT or AOS).

Extended microscopic three temperature model:

As discussed before, from the experimental observations we have eliminated spin current as well as dipolar field and argued that RKKY exchange coupling is the mechanism for the switching phenomena of Co/Pt multilayers. In this section, we will explain RKKY exchange coupling mediated HI-AOS dynamics by extending the microscopic three temperature model (M3TM) proposed by Beens et al.[17,18] The details of the model is discussed below with further details to be published elsewhere.[27] Basically, we solve a set of differential equations for electron and phonon sub-systems for both the $Co_{70}Gd_{30}$ alloy and Co/Pt multilayer according to the two-temperature model (2TM), including the heat dissipation through the substrate, to calculate electron and phonon temperatures (T_e and T_l) as a function of time (see supplementary section S5). Note that Co/Pt multilayers are considered as a single layer in the simulation. The laser pulse energy, expressed by a gaussian function with FWHM of 100 fs, is absorbed by the electron system. The absorbed optical energy by the Co/Pt ML and the $Co_{70}Gd_{30}$ alloy is calculated by the transfer matrix method[28] using the optical constants tabulated in Table 1 of supplementary note S3 and the measured thicknesses of each of the layers. The electron and phonon systems are respectively described by a spin-less free electron gas and Debye models. The spin sub-systems of CoGd (Co and Gd sublattices) and Co/Pt multilayers are modeled according to Weiss mean field theory assuming the spin quantum number S_i = 1/2. As explained by Beens et al., we have considered two channels for spin angular momentum transfer for CoGd. The electron-electron exchange scattering between Co and Gd sublattices and Elliot-Yafet spin-flip scattering due to electron-phonon interaction. In addition to these, one extra channel is added due to long range RKKY exchange coupling with the Co/Pt multilayers. For the Co/Pt multilayer only Elliot-Yafet type spin relaxation process and RKKY type long range exchange scattering are considered. Hence the exchange splitting parameters are expressed as

$$\Delta_{Co} = x\gamma_{Co-Co}m_{Co} + (1-x)\gamma_{Co-Gd}m_{Gd} + \frac{(\gamma_{CoPt-Co}m_{CoPt})}{4}$$
$$\Delta_{Gd} = x\gamma_{Gd-Co}m_{Co} + (1-x)\gamma_{Gd-Gd}m_{Gd} + \frac{(\gamma_{CoPt-Gd}m_{CoPt})}{4}$$
$$\Delta_{CoPt} = \gamma_{CoPt-CoPt}m_{CoPt} + \frac{\gamma_{CoPt-Co}m_{Co}}{4} + \frac{\gamma_{CoPt-Gd}m_{Gd}}{4},$$

where $\gamma_{ij} = zJ_{ij}\mu_j\,; (i,j \in \{Co, Gd, Co/Pt\})$. The exchange coupling parameter $J_{ii} = \frac{3k_BT_{c,i}}{2zS_i(S_i+1)}, i = \{Co, Gd, CoPt\}$. Here $z = 12$ is the number of next nearest neighbors considering an FCC type of lattice and $T_{c,i}$ is the Curie temperature of individual elements $\left(T_{c,co} = 1400\ K,\right.$ $\left.T_{c,Gd} = 292\ K\ and\ T_{c,Co/Pt} = 580\ K\right)$. The antiferromagnetic inter-sublattice exchange coupling parameter is taken to be, $J_{Co-Gd} = -0.388 \times J_{Co}$.[17] The last terms of the first two equations and the last two terms of the third equation describes the RKKY exchange interaction for which the Co/Pt multilayers is approximated as a single layer. The RKKY coupling strength (J_{RKKY}) has been varied up to 5% of direct exchange of Co/Pt, i.e $J_{RKKY} = \pm(0\ to\ 0.05) \times J_{CoPt} = \pm(0\ to\ 6.658) \times 10^{-23}$ J. The sign defines the type of RKKY coupling (ferromagnetic or anti-ferromagnetic), which is controlled by the thickness of the spacer layer (Pt in our case for example). With this model we simulated three types of ferromagnet-ferrimagnet heterostructures such as ferromagnetically coupled (Pt spacer 1 nm), antiferromagnetically coupled (Pt spacer 3nm) and decoupled (Pt spacer 4 nm). The absorbed laser energy by the respective magnetic layers for these three types of samples are calculated by the transfer matrix method. Figure 5 describes the switching dynamics at the minimum absorbed energy, for these three heterostructures. The RKKY coupling strength is considered to be $J_{RKKY} = \pm 0.05 \times J_{CoPt}$ for Figure 5a, b and c, d respectively representing ferromagnetic and antiferromagnetic coupling. There is no sharp change observed in the electronic temperature after 3.5 ps (2 ps) for Co/Pt (CoGd) subsystem. After 4 ps, the electron temperature of Co/Pt (CoGd) gets reduced to 450 K (985 K) as shown in the temperature profile of Fig. 5. It has been theoretically predicted that RKKY coupling amplitude is reduced by ~18 % at a temperature of 750 K.[29] Hence, we have used room temperature amplitude of RKKY coupling and assumed it to be temperature independent. The dynamics calculated with our model exhibits magnetization reversal of CoGd irrespective of coupling (see Figure 5a,c and e) similar to our experimental observation. CoGd exhibits switching in 1.5 ps, which is in agreement with experiment. Moreover, Co/Pt MLs exhibit switching for both ferromagnetic and antiferromagnetic coupling as shown in Figure 5b and d. For the decoupled case, the magnetization of Co/Pt undergoes sharp demagnetization followed by slow recovery along its initial direction as shown in Figure 5f, however the ferrimagnet switches as shown in Figure 5e. For ferromagnetic and antiferromagnetically coupled samples, we observe that Co/Pt switches in a two-step like process. First a fast (due to its smaller atomic magnetic moment compared to Co or Gd) and almost full demagnetization at ~450 fs, and then switching at ~4 ps, which is close to the experimental switching time. The two step switching process is also in agreement with the present and also previous measurements[15], which is a signature of exchange mediated switching. Our simulation shows that the electron temperature of Co/Pt increases with the incident laser energy, and it takes a longer time to cool down below the Curie temperature (See Figure S6). As a result, Co/Pt stays in demagnetized state until it is cooled down and the RKKY exchange acts on it from the already switched CoGd via RKKY exchange coupling. Since Co/Pt stays close to fully demagnetized state before switching, we calculate the switching time when its magnetization crosses a small positive value (0.01) to avoid any ambiguity. The switching time of Co/Pt depends significantly on absorbed laser energy and the strength of RKKY coupling, which is shown in Figure 6. The switching becomes faster with the increase in RKKY strength and slower as a function of absorbed energy. With increasing RKKY strength, it is obvious that the Co/Pt layer gets enough angular momentum (from the CoGd subsystem) to switch on a much faster timescale. On the other hand, upon increasing the laser energy, the maximum lattice temperature of Co/Pt linearly increases with the absorbed optical energy. As we increase the incident/absorbed energy, the difference between the Currie temperature and the maximum lattice temperature decreases. Therefore, the Co/Pt moments spend longer time in the demagnetized state before they are flipped in the opposite direction, resulting in slower switching dynamics of Co/Pt.

In conclusion, we have experimentally demonstrated RKKY exchange coupling mediated ultrafast all-optical switching of a Co/Pt MLs exchange coupled with a CoGd alloy. Layer resolved single-shot imaging has revealed HI-AOS of Co/Pt multilayers for both ferromagnetic and antiferromagnetic type of RKKY coupling. The switching speed of Co/Pt multilayers ferromagnetically coupled with CoGd by 1nm Pt spacer is ~3 ps, which is the fastest switching of a ferromagnet ever reported.[15,30] Theoretical simulation using extended microscopic three temperature model resulted in temporal magnetization dynamics consistent with the experimental dynamics. The simulated dynamics unveils AOS switching speed of CoGd and Co/Pt multilayers to be ~1.5 ps and ~4 ps respectively. The dynamics of the Co/Pt multilayers depends on the absorbed laser energy and the strength of RKKY coupling. The switching becomes slower upon increasing the incident/absorbed laser energy and faster with the RKKY exchange energy. Thereby, this investigation lays the foundation of combinatorial experimental-theoretical understanding for engineering a RKKY exchange coupled ferromagnet-ferrimagnet heterostructure for picosecond opto-magnetic memory applications.

Acknowledgements

This work was primarily supported by the Director, Office of Science, Office of Basic Energy Sciences, Materials Sciences and Engineering Division, of the U.S. Department of Energy under Contract No. DE-AC02-05-CH11231 within the Nonequilibrium Magnetic Materials Program (MSMAG). This work was also supported by ASCENT (one of the SRC/DARPA supported centers within the JUMP initiative) (data acquisition). We also acknowledge support by the National Science Foundation Center for Energy Efficient Electronics Science (data analysis).

Author contribution

JC designed the experiment with inputs from JB. JC optimized and deposited the samples by sputtering and characterized by MOKE microscopy. JC conducted the AOS characterization by laser with contribution from AP. DP performed simulation with contribution from HJ and JC. JC analyzed the experimental and simulation results together with JB and DP. JC wrote the manuscript with input from all the authors.

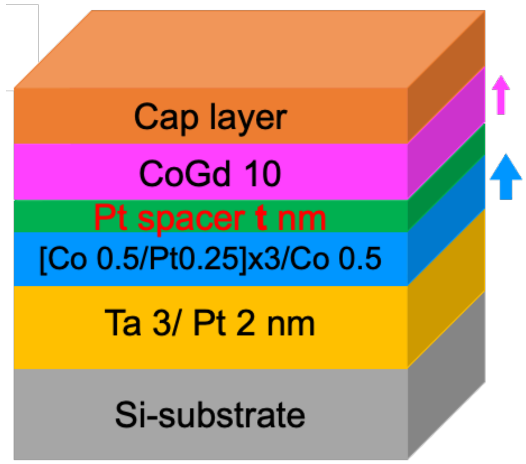

Figure 1: Schematic diagram of the layer configuration of the samples used for this investigation. The blue and pink arrows respectively represent the magnetization direction of Co/Pt multilayers and CoGd ferrimagnetic alloy

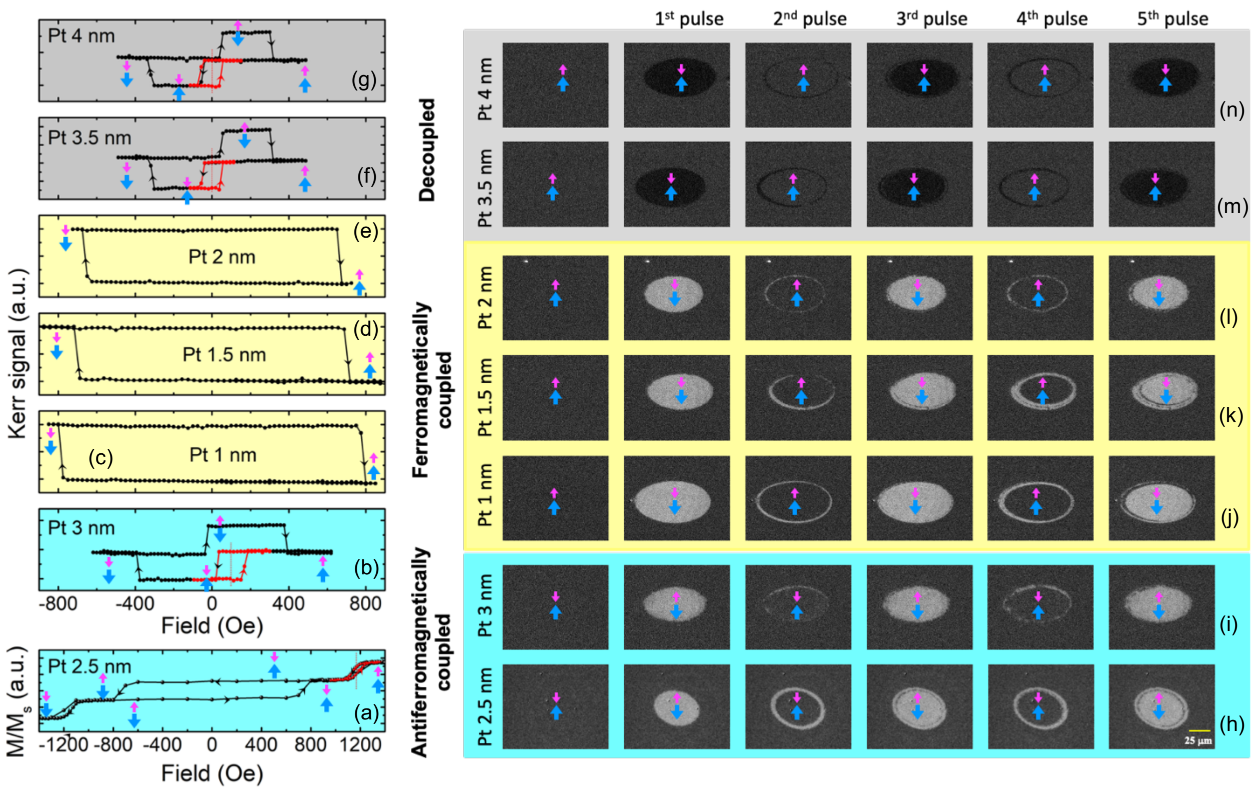

Figure 2: Out-of-plane magnetic hysteresis loops measured by (a) vibrating sample magnetometry (b-g) MOKE microscopy of the heterostructures shown in figure 1 for different Pt-spacer thicknesses from 1 to 4 nm with 0.5 nm steps. (h-n) Single shot HI-AOS MOKE images of the corresponding stacks with different spacer thicknesses. The hysteresis loops and single-shot switching images on grey, yellow and cyan shaded regions are respectively for the decoupled, ferromagnetically coupled and anti-ferromagnetically coupled samples. The red color loops are the minor loops of CoGd.

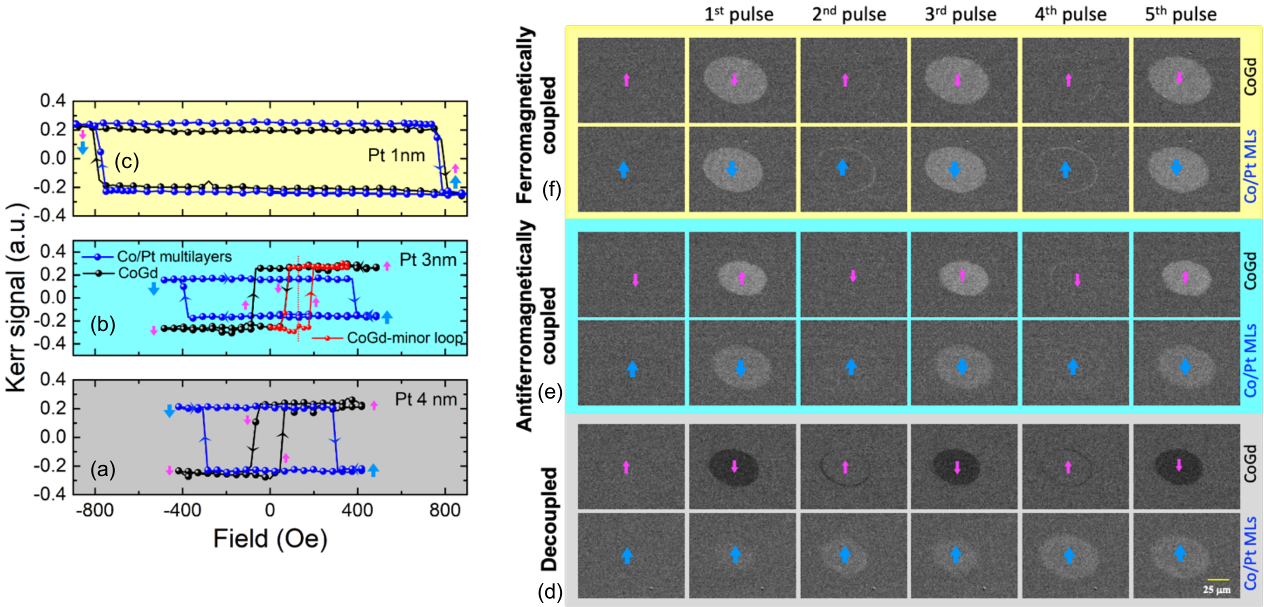

Figure 3: Layer-sensitive (a-c) magnetic hysteresis loops and (d-f) single shot HI-AOS images of three types of exchange coupled stacks {[Co 0.5/Pt 0.25]$_3$/Co 0.5/ Pt (1, 3, 4)/ CoGd 10 nm} measured by MOKE microscopy. The hysteresis loops and single-shot switching images on grey, yellow and cyan shaded regions are respectively for the decoupled, ferromagnetically coupled, anti-ferromagnetically coupled samples. The black and blue color hysteresis loops are measured when the MOKE is sensitive to CoGd and Co/Pt multilayers respectively. Shifted red color loop for Pt 3 nm spacer is the minor loop of CoGd suggesting antiferromagnetic RKKY exchange bias. First row and second row of single-shot switching images respectively represent the switching of CoGd-alloy and Co/Pt multilayers for three different samples.

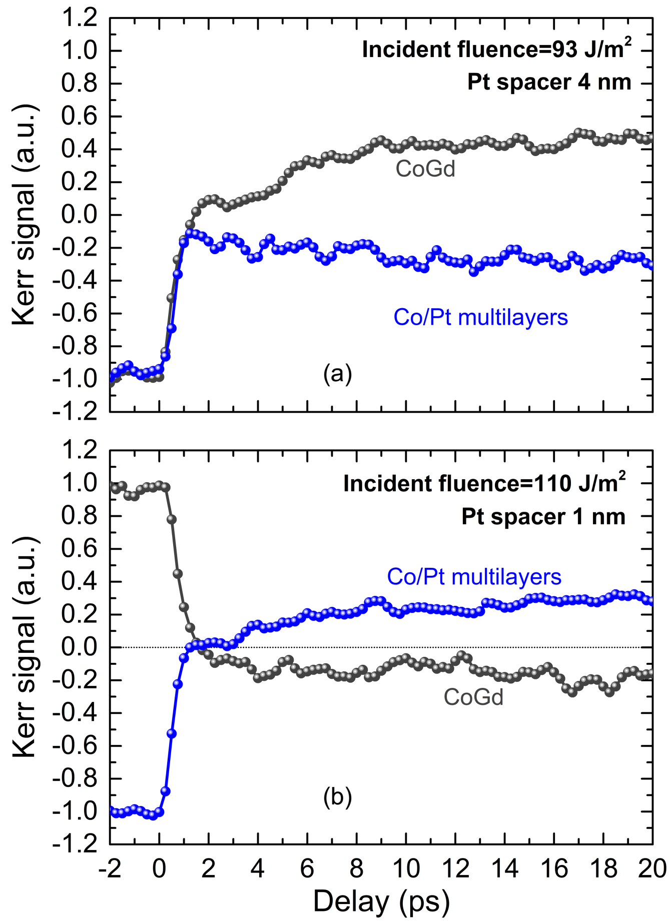

Figure 4: Depth-sensitive time-resolved magnetization dynamics of CoGd alloy and Co/Pt multilayers of (a) decoupled stack with 4 nm Pt spacer and (b) ferromagnetically coupled stack with 1 nm Pt spacer.

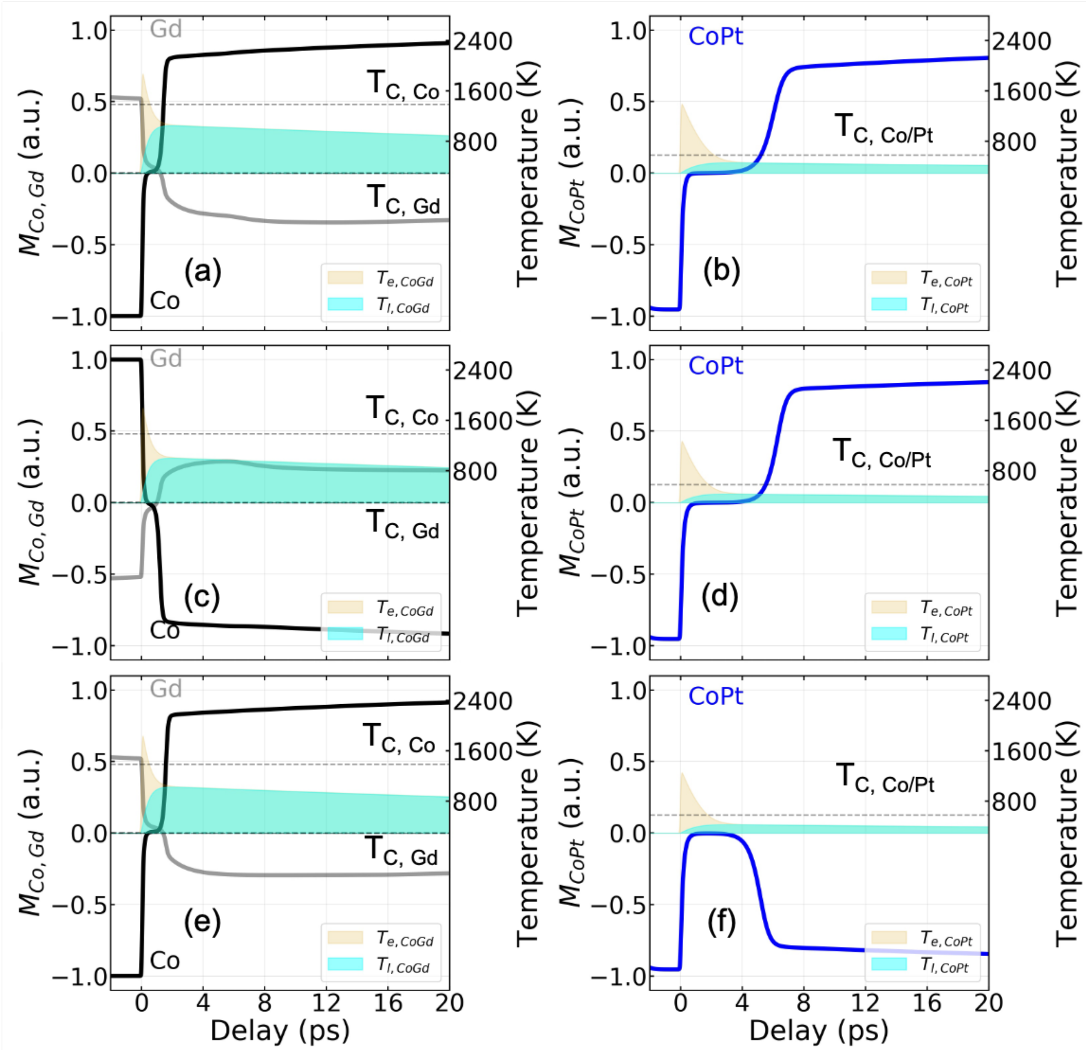

Figure 5: Temporal dynamics of exchange coupled heterostructures obtained from extended-M3TM model. Magnetization dynamics of (a,b) ferromagnetically coupled system with Pt 1 nm spacer, (c,d) antiferromagnetically coupled system with Pt 3 nm spacer, and (e,f) decoupled system with Pt 4 nm spacer. The yellow and cyan shaded regions respectively represent electron and lattice temperatures as a function of pump-probe delay. The dashed lines are the Currie temperature of the Co (1400 K), Gd (292 K) and Co/Pt (580 K) sub-lattices.

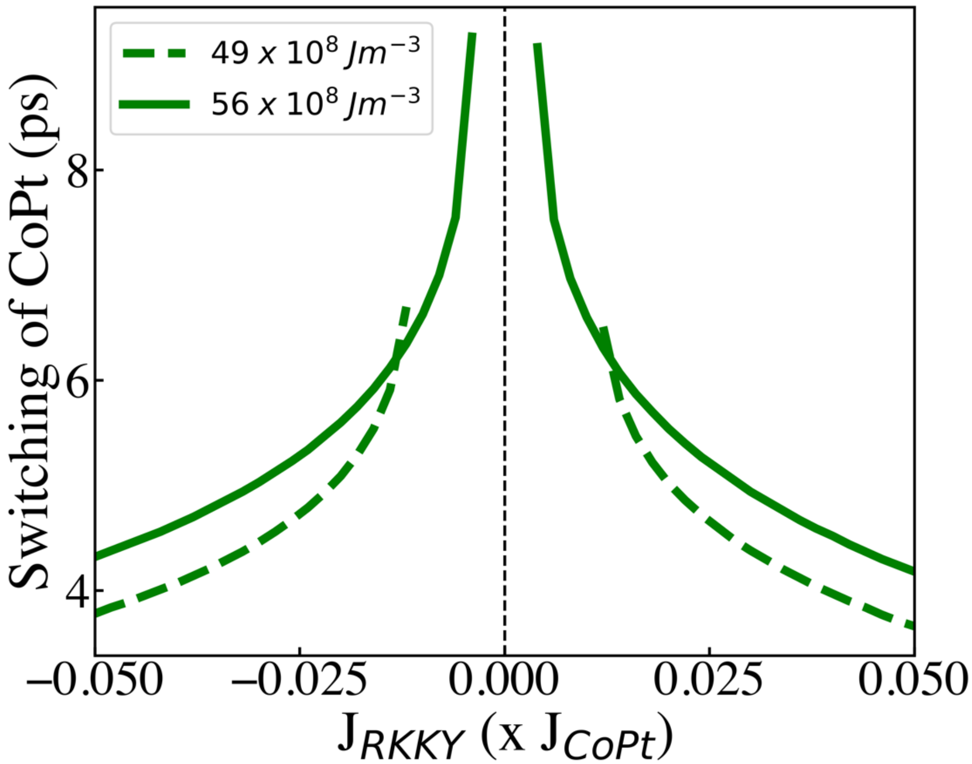

Figure 6: Switching time of Co/Pt as a function of RKKY exchange strength for both ferromagnetic and antiferromagnetic coupling at two different absorbed optical energies.

[1] E. Beaurepaire, J. C. Merle, A. Daunois, J. Y. Bigot, *Phys. Rev. Lett.* **1996**, *76*, 4250.

[2] C. D. Stanciu, A. Tsukamoto, A. V. Kimel, F. Hansteen, A. Kirilyuk, A. Itoh, T. Rasing, *Phys. Rev. Lett.* **2007**, *99*, 14.

[3] T. A. Ostler, J. Barker, J. Mentink, E. Mengotti, A. M. Kalashnikova, U. Atxitia, B. A. Ivanov, S. El Moussaoui, A. Kirilyuk, O. Chubykalo-Fesenko, L. J. Heyderman, R. F. L. Evans, A. Tsukamoto, A. V. Kimel, L. Le Guyader, F. Nolting, T. Rasing, A. Itoh, K. Vahaplar, R. W. Chantrell, D. Afanasiev, *Nat. Commun.* **2012**, *3*, 666.

[4] I. Radu, K. Vahaplar, C. Stamm, T. Kachel, N. Pontius, H. A. Dürr, T. A. Ostler, J. Barker, R. F. L. Evans, R. W. Chantrell, A. Tsukamoto, A. Itoh, A. Kirilyuk, T. Rasing, A. V. Kimel, *Nature* **2011**, *472*, 205.

[5] Y. Yang, R. B. Wilson, J. Gorchon, C. H. Lambert, S. Salahuddin, J. Bokor, *Sci. Adv.* **2017**, *3*, e1603117.

[6] D. Sander, S. O. Valenzuela, D. Makarov, C. H. Marrows, E. E. Fullerton, P. Fischer, J. McCord, P. Vavassori, S. Mangin, P. Pirro, B. Hillebrands, A. D. Kent, T. Jungwirth, O. Gutfleisch, C. G. Kim, A. Berger, *J. Phys. D. Appl. Phys.* **2017**, *50*, 363001.

[7] E. Y. Vedmedenko, R. K. Kawakami, D. D. Sheka, P. Gambardella, A. Kirilyuk, A. Hirohata, C. Binek, O. Chubykalo-Fesenko, S. Sanvito, B. J. Kirby, J. Grollier, K. Everschor-Sitte, T. Kampfrath, C. Y. You, A. Berger, *J. Phys. D. Appl. Phys.* **2020**, *53*, 453001.

[8] A. El-Ghazaly, B. Tran, A. Ceballos, C.-H. Lambert, A. Pattabi, S. Salahuddin, F. Hellman, J. Bokor, *Appl. Phys. Lett.* **2019**, *114*, 232407.

[9] A. Ceballos, A. Pattabi, A. El-Ghazaly, S. Ruta, C. P. Simon, R. F. L. Evans, T. Ostler, R. W. Chantrell, E. Kennedy, M. Scott, J. Bokor, F. Hellman, *Phys. Rev. B* **2021**, *103*, 24438.

[10] M. L. M. Lalieu, M. J. G. Peeters, S. R. R. Haenen, R. Lavrijsen, B. Koopmans, *Phys. Rev. B* **2017**, *96*, 220411(R).

[11] L. Avilés-Félix, L. Álvaro-Gómez, G. Li, C. S. Davies, A. Olivier, M. Rubio-Roy, S. Auffret, A. Kirilyuk, A. V. Kimel, T. Rasing, L. D. Buda-Prejbeanu, R. C. Sousa, B. Dieny, I. L. Prejbeanu, *AIP Adv.* **2019**, *9*, 125328.

[12] C. Banerjee, N. Teichert, K. E. Siewierska, Z. Gercsi, G. Y. P. Atcheson, P. Stamenov, K. Rode, J. M. D. Coey, J. Besbas, *Nat. Commun.* **2020**, *11*, 4444.

[13] J. Y. Chen, L. He, J. P. Wang, M. Li, *Phys. Rev. Appl.* **2017**, *7*, 021001.

[14] S. Iihama, Y. Xu, M. Deb, G. Malinowski, M. Hehn, J. Gorchon, E. E. Fullerton, S. Mangin, *Adv. Mater.* **2018**, *30*, 1804004.

[15] J. Gorchon, C. H. Lambert, Y. Yang, A. Pattabi, R. B. Wilson, S. Salahuddin, J. Bokor, *Appl. Phys. Lett.* **2017**, *111*, 042401.

[16] K. Cai, Z. Zhu, J. M. Lee, R. Mishra, L. Ren, S. D. Pollard, P. He, G. Liang, K. L. Teo, H. Yang, *Nat. Electron.* **2020**, *3*, 37.

[17] M. Beens, M. L. M. Lalieu, A. J. M. Deenen, R. A. Duine, B. Koopmans, *Phys. Rev. B* **2019**, *100*, 220409(R).

[18] M. Beens, M. L. M. Lalieu, R. A. Duine, B. Koopmans, *AIP Adv.* **2019**, *9*, 125133.

[19] J. Chatterjee, S. Auffret, R. Sousa, P. Coelho, I. L. Prejbeanu, B. Dieny, *Sci. Rep.* **2018**, *8*, 11724.

[20] A. J. Schellekens, N. De Vries, J. Lucassen, B. Koopmans, *Phys. Rev. B* **2014**, *90*, 104429.

[21] T. Lichtenberg, Limitations and possibilities of the layer specific moke setup, Eindhoven University of Technology, **2015**.

[22] M. Hofherr, P. Maldonado, O. Schmitt, M. Berritta, U. Bierbrauer, S. Sadashivaiah, A. J. Schellekens, B. Koopmans, D. Steil, M. Cinchetti, B. Stadtmüller, P. M. Oppeneer, S. Mathias, M. Aeschlimann, *Phys. Rev. B* **2017**, *96*, 100403(R).

[23] S. Pan, O. Hellwig, A. Barman, *Phys. Rev. B* **2018**, *98*, 214436.

[24] Y. L. W. van Hees, P. van de Meugheuvel, B. Koopmans, R. Lavrijsen, *Nat. Commun.* **2020**, *11*, 3835.

[25] G. M. Choi, C. H. Moon, B. C. Min, K. J. Lee, D. G. Cahill, *Nat. Phys.* **2015**, *11*, 576.

[26] G. M. Choi, B. C. Min, *Phys. Rev. B* **2018**, *97*, 014410.

[27] D. Polley, J. Chatterjee, H. Jang, J. Bokor, *to be Publ.*

[28] L. Alber, V. Scalera, V. Unikandanunni, D. Schick, S. Bonetti, *Comput. Phys. Commun.* **2021**, *265*, 107990.

[29] A. Kundu, S. Zhang, *J. Magn. Magn. Mater.* **2015**, *393*, 331.

[30] E. Grimaldi, V. Krizakova, G. Sala, F. Yasin, S. Couet, G. Sankar Kar, K. Garello, P. Gambardella, *Nat. Nanotechnol.* **2020**, *15*, 111.